Inter- and intra-observer variability of left ventricular hemodynamic forces derived from feature-tracking cardiac magnetic resonance.

Student: Temirlan Ismailov

Supervisor: Alessandro Salustri, MD, PhD

Bachelor of Medical Sciences

Nazarbayev University School of Medicine

Astana, 2023

DECLARATION:

I hereby declare that the Capstone project is my original work, and it has been written by me in its entirety. I have duly acknowledged all the sources of information that have been used in the Capstone project. In addition, this Capstone project has also not been submitted for any degree in any university previously.

Abstract

Hemodynamic forces (HDF) analysis represents a novel approach to quantify intraventricular pressure gradients (IVPG). Recently, a new noninvasive method for evaluating HDF based on feature tracking has been proposed, however data on the reproducibility of this method is still scanty. Thus, the aim of this study is to assess the reproducibility of HDF parameters derived from cardiac magnetic resonance (CMR).

Twenty athletes' CMR studies were analyzed by two independent observers and 15 of them were re-analyzed by the same observer one week apart. Intraclass Correlation Coefficient and Bland-Altman plots were used to assess association and agreement of the Longitudinal HDF (A-B), Transverse HDF (L-S), and Impulse Angle. For two different observer measurements, there was a good association for the A-B and L-S (ICC 0.82 and 0.85, respectively; $p<0.001$), and quite a good association for the Impulse Angle (ICC 0.67; $p<0.012$). For the same observer's measurements one week apart, the ICC values for A-B, L-S, and Impulse Angle showed excellent correlation and high statistical significance (0.89, 0.93, and 0.82, respectively; $p<0.001$).

The results of this study showed a low inter- and intra-observer variability of HDF parameters derived from CMR.

Introduction

The analysis of myocardial function has been based so far on the evaluation of left ventricular wall motion (either regional or global) (Reddy et al., 2015) or on the velocity of the blood within the heart (Doost et al., 2016), which are both surrogates of the intrinsic myocardial contractile properties. In fact, the development of intraventricular pressure gradients is responsible for blood flow within the heart and large vessels (Flachskampf et al., 2015). Recently, the quantification of intraventricular pressure gradients using hemodynamic forces (HDF) analysis has been proposed as a new approach for a complete assessment of cardiac hemodynamics and for analyzing the strength with which blood propagates within the left ventricle (LV) (Thomas and Popović, 2005). The importance of new parameters for detecting LV dysfunction is related to the limitations of the current methods, both for systolic as well as diastolic dysfunction. For example, LV ejection fraction (EF) is based on volume ratios (and not on the intrinsic myocardial contractile state), strain evaluates myocardium only (not the dynamic of the blood), and Doppler methods for assessing LV diastolic dysfunction are flow-dependant (Airale et al., 2021). Thus, it is important to highlight the physiological significance and the potential clinical relevance of HDF analysis, which could lead to the early detection of LV systolic and diastolic dysfunction.

HDF can be analyzed, either with ultrasound or cardiac magnetic resonance (CMR) imaging, using two different approaches (Vallelonga, et al., 2021). Previous methods were based on flow analysis, specifically using particle velocimetry ultrasound imaging (Pedrizzetti et al., 2016) and four-dimensional flow magnetic resonance imaging (Eriksson et al., 2015). However, this approach has been heavily hampered by the use of contrast agents and the lack of widespread availability in clinical practice. Recently, the application of a new mathematical model to speckle tracking (a visual pattern from the interference between the ultrasound beams and the myocardium surface) allowed for the echocardiographic analysis of the HDF independent from the flow with the potential of an easier application in clinical settings (Claus et al., 2015). This approach can also be translated to feature tracking CMR. Tracking is a methodology that follows the distinct elements of an image when these are present in consecutive frames. A distinct element, in general, is a “feature” made by the combination of anatomical and texture elements of the image. In the echocardiographic images, these features are equivalent to speckles. Thus, the term “feature” applies to echocardiography and magnetic resonance imaging, while the term “speckle” is the feature that is most pertinent to echocardiography (Pedrizzetti et al., 2016). In terms of potential clinical application, HDF could provide new insights into the interaction between flow and tissue, with abnormal HDF resulting in LV development and remodeling (as demonstrated by an embryological study by Hove et al., 2003) and conversely LV dysfunction into abnormal flow. Although early detection of such cardiac structural abnormalities in asymptomatic patients is an attractive application of HDF analysis, more systematic research is needed to support this hypothesis. More specifically, HDF should be studied in patients with cardiovascular pathologies and represented in a way that would help physicians understand how to interpret HDF information and decide whether to proceed with treatment (Midgett et al., 2014). Furthermore, this method could be ideally applied to follow-up studies in patients with chronic heart disease (post-myocardial infarction, heart valve disease, cardiomyopathies, hypertensive heart disease, heart failure) for detection of subtle changes in cardiac function and hemodynamics. However, a reliable comparison of studies in a given patient at different times requires variability of the measurements as low as possible to differentiate between

real changes due to the progression of the disease and artificial changes due to the variability of the measurements. Unfortunately, despite the great potential interest for HDF analysis, its wide acceptance and clinical relevance need solid data on the variability which are still lacking (Anvari et al., 2018).

An example of the importance of variability is the measurement of the body temperature using a mercury thermometer in clinical practice (Sund-Levander et al., 2004). Looking at the thermometer, the scale should be clear and detailed enough to provide the same interpretation by different individuals (inter-observer variability) and by the same individual in two different readings (intra-observer variability). The variability of any measurement must be taken into consideration when interpreting the results of any method, thereby establishing an accepted range of difference in readings and interpretation.

A more quantitative example is the variability of the left ventricular endocardial border tracing of the echocardiographic or CMR images. While most of the softwares provide an automatic tracing, the observers have the freedom to manually tweak the border tracing trajectory depending on their visual judgment of the tracing accuracy (Monosilio et al., 2022). In other words, the analysis of cardiac images introduces another source of variability that is related to the inevitable human factor that is intrinsically present in such measurements (Popovic and Thomas, 2017). In fact, most of the parameters derived from echocardiographic or CMR images require either a subjective assessment or a manual interaction between the observer and the images, as it is in the case of linear measurements or border tracing (Szulik et al., 2011). Clearly, in order to have a clinical application, parameters measured on the same image should not differ significantly both among several observers (inter-observer variability) and between the same observer on two occasions apart (intra-observer variability) (Meesters et al., 2020).

With these concepts in mind, we sought to assess the inter- and intra-observer variability of the HDF parameters derived from feature tracking CMR. This assessment is a pre-requisite for the validation of the robustness of this method and will likely open new avenues for its application in clinical settings. Considering the experience of the observers in cardiac imaging and the mostly automatic image analysis of the software we have used, we hypothesized that there will be high reproducibility. Still, if the degree of reproducibility is low, insight for further research methodology will be established. Moreover, we sought to determine the relative weight in terms of variability of the several steps of HDF analysis.

Materials and Methods

Study Population

This research is part of an ongoing study that evaluates the effect of intense physical training on HDF in athletes. Briefly, athletes will undergo CMR at the end of the off-season and the HDF parameters derived from the CMR images will be compared with those obtained after three and six months of intense physical training and with those obtained in a group of patients with longstanding hypertension. The study was approved by the Ethical Committee of Nazarbayev University (NU-IREC #550/20042022).

For the purpose of this study, 20 endurance athletes were randomly selected and analyzed for inter- observer variability and 15 of them were checked for intra- observer variability.

Cardiac MR acquisition

Cine CMR studies were performed at the National Research Cardiac Surgery Center in Astana, Kazakhstan, using a Siemens Magnetom Avanto 1.5 Tesla machine. The CMR scanning protocol was based on the "Cardiovascular Magnetic Resonance Pocket Guide" *(Bernhard et al., 2017)*. The localizer scans were acquired using TRUFI (True Fast Imaging with Steady-State Free Precession), multi two-chamber view, IPAT (Institute for Personality and Ability Testing), and four-chamber view. These were followed by white-blood image acquisitions in long axis four-, two-, and three-chamber, and short-axis views. For all acquisitions, the distance factor was kept at 20% with slice thickness of 8 mm. Upon acquisition, all the images were stored in the Picture Archiving and Communication System (PACS) and retrieved for off-line analysis.

Analysis of CMR images

Images were analyzed by two independent observers with more than six years of experience in cardiac imaging. CMR images were analyzed using a dedicated software (Q Strain version 1.3.0.79; Medis, Leiden, the Netherlands) which allows to calculate HDF by visualizing three routine long-axis and one short-axis cine randomly pre-selected images from PACS. The algorithm is based on a mathematical model developed by Pedrizzetti et al. (2015):

$$V(t)\,F\,(t) = Z\,S(t)\,\rho vvndS + Z\,V(t)\,\rho\,\partial v\,\partial t\,dV \qquad (1)$$

The calculation of the LV HDF requires measurements of the mitral valve and aortic valve area. The mitral valve area was calculated from the measurement of the mitral annulus diameter ($A = \pi\,[d/2]^2$) and the measurements were performed only after the observers selected the appropriate cardiac frame with maximal mitral valve opening. Mitral valve area was calculated from the four-chamber and two-chamber views and the mean of the two values were considered. Due to the absence of aortic valve obstruction, the aortic valve area was derived from the LV outflow tract (OT) area in the three-chamber view. LVOT area was calculated from the LVOT diameter using the

same principle that was used for the MV area. For each structure (MV and LVOT), three measurements of the diameters were performed and the values were averaged and inserted manually into the software for automatic calculation of the mitral valve and LVOT area.

Left ventricular endocardial border was then automatically detected by the software after the observer chose the appropriate cardiac images. With the help of the software's endocardial contouring feature, the Global Longitudinal Strain (GLS), an index of myocardium deformation, was calculated. It is important to note that the observers were able to manually change the automatic endocardial borders selected by the program, if needed. In cases when the detection of End-Systole (ES) and End-Diastole (ED) time points was not performed automatically, the observers could select those time-points by looking at consecutive cardiac frames on each long-axis view. In addition, according to standard practice, standard volumetric parameters (such as the LV volumes and ejection fraction) were derived.

Before starting this study, three joint reading sessions on analysis of clinical routine CMR studies were conducted for standardization of measurements between the two observers.

The main steps of HDF analysis are summarized in **Figure 1**.

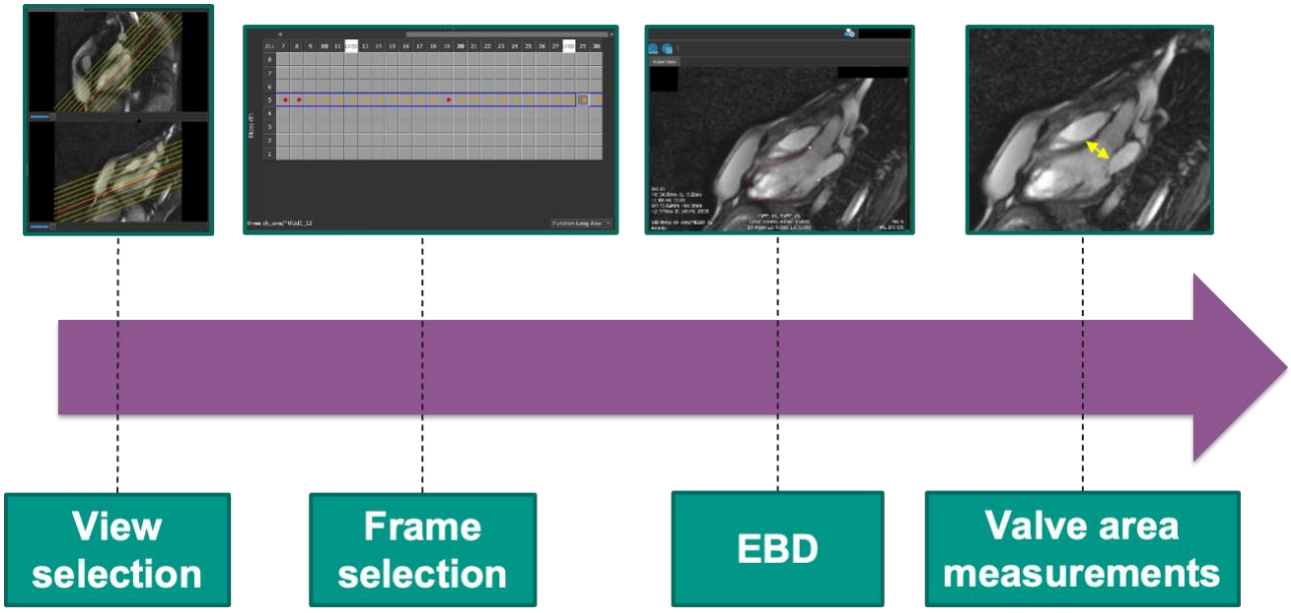

Figure 1

The main steps of HDF analysis. First, the observer selects and then imports the CMR images. Then, the observers scrolls the cardiac loop to select the "best" frame. At this point, the software automatically performs the endocardial border detection for feature-tracking manually, however the operator has the freedom to manual adjustment, if needed. Finally, aortic and mitral valve diameter are measured for valve area assessment.

HDF parameters

In the normal LV, HDF occurs in the apical-base (A-B) and lateral-septal (L-S) planes, with the A-B direction being the most predominant force. According to (Laenens et al., 2023), the A-B direction of the forces is depicted as a curve that deflects positively when HDF is directed toward the LV base and negatively when it is directed toward the LV apex. The Newton (N) is the unit of force. Typically, the root mean square, which includes both positive and negative values, is used to express the amplitude characteristics of HDF. The value of HDF is divided by the fluid density and gravity acceleration after being initially normalized to the equivalent LV volume. This makes it possible to describe the acceleration due to gravity as a percentage (dimensionless) and makes it easier to compare subjects. Furthermore, the angle designating the dominant force vector during the entire cardiac cycle (ranging from 0° to 360°) was calculated to express the orientation parameters of HDF (**Figure 2**) (Filomena et al., 2021).

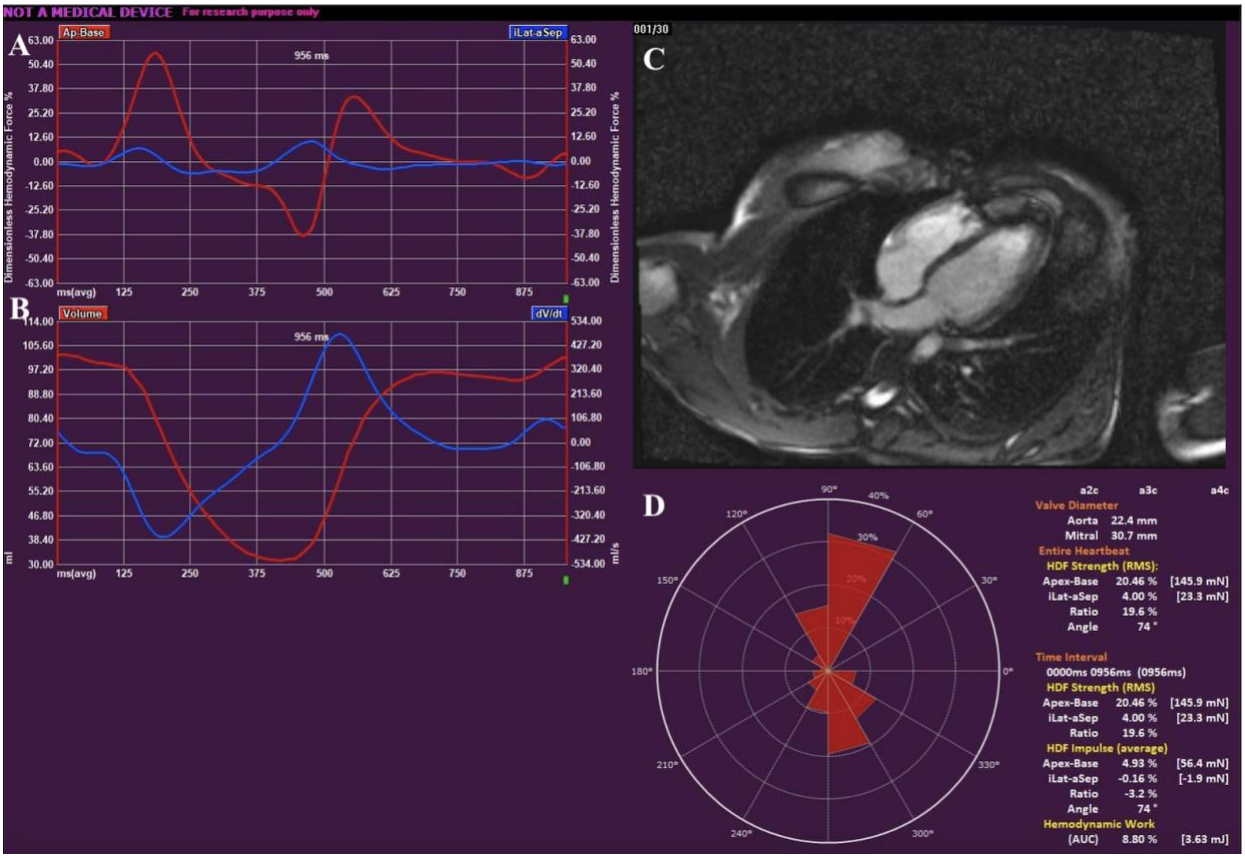

Figure 2.

HDF parameters curve (Panel A, A-B in red; L-S in blue); LV volume and rate of changes in LV volume curve (Panel B); Cardiac MRI image (Panel C); Polar histogram (Panel D) depicting the distribution and magnitude of LV HDFs. The magnitude (red triangles) and directional distribution (angles) of HDF across the entire heart cycle are both depicted on a polar histogram. The top of the

histogram (90 degrees) is used to symbolize the LV base, while the bottom (270 degrees) is used to indicate the LV apex.

In addition to HDF, Global Longitudinal Strain (GLS) and Global Circumferential Strain (GCS) was also considered through the CMR feature tracking technique, which involved the application of a particular algorithm on the patterns of cine images.

Variability assessment

The association, bias, and agreement were quantified and interpreted according to the (Bunting, et al., 2019) guide, which recommends the Intra Class Coefficient (ICC), Bland-Altman plots, and t-test respectively. ICC values in the 0.75-1.00 range suggested excellent correlation, and those in the 0.60-0.74 indicated good correlation (Bunting, et al., 2019).

Data storage and data security

The collected data was made anonymous. Health records were handled according to Kazakhstan's Law on Protected Personal Information (PPI). In accordance with the Kazakhstani law, best practices, and Nazarbayev University's Institutional Research and Ethics Committee (IREC) policy requirements, all personally identifiable information was deleted, and demographic data was anonymized. All data was available to researchers and study team members who have received IREC approval. On a dedicated workstation, extracted data was processed and analyzed.

Ethical considerations

Both image and data analysis were used in this study. The IREC of Nazarbayev University received all trial protocols, processes, data gathering, and storage. Each participant in the study has given their informed consent, and all information gathered and findings are being kept private. Each participant in the study was given an ID number, and all hard copies of the data gathered or used are being kept in a cabinet in the study staff's closed office. Also, all electronic data is being kept on the research staff's password-protected computers in their secured offices and personnel facility. All of these patient files were only accessible to necessary research professionals.

Results

The general characteristics of the athletes analyzed by the two observers are visualized in **Table 1**. The gender was equally distributed, the mean age was 30.0 ± 9.1 years, and the mean length of experience in sport was 11.4 ± 8.3 years. Furthermore, heart rate, systolic and diastolic blood pressure were in the normal range.

Inter-observer variability

For the cardiac frame selection, a difference of ≤2 frames between the two observers was present in 92% of the cases and in 100% of the cases re-analysed by the same observer one week apart.

Volumetric, valve diameter, strain, and HDF parameters for the 20 athletes are shown in **Table 2**. Pearson's correlation coefficient was used to assess a linear correlation between two-independent continuous variables. The values provided by the two observers showed a high statistically significant correlation ($p<0.001$ for all parameters).

Valve diameter

ICC test was used to rule out the bias of repeated measurements of continuous variables. While the aortic valve area showed a good correlation between different observer measurements (ICC=0.68; $p<0.001$), these results were even stronger and more significant for the mitral valve area (ICC=0.82; $p<0.001$) (**Table 2**).

Global Longitudinal Strain

Similarly, the ICC values of endocardial GLS (GLS-endo) followed the same trend (ICC 0.82; $p<0.001$) (**Table 2**).

HDF

Although the volumetric, valve area, and strain parameters are relevant and form the background for further analysis, the main aim of this study was to assess the variability of the HDF parameters. Overall, the ICC values and p-values showed an acceptable bias of all the HDF variables [A-B (0.82 and <0.001), L-S (0.85 and <0.001), and Impulse Angle (0.67 and =0.012)] (**Table 2**).

Scatter plots showing the correlation between the HDF parameters can be visualized in **Figure 3**. The correlation between the two observers can be judged by the general pattern of the data points, which all created a clear pattern of correlation for the three HDF parameters through the noticeable line of best fit. While the slope for the A-B HDF was 0.72 and the one for the Impulse Angle was 0.67, and the slope for the L-S HDF was 0.89. These results indicate minimal proportional bias and no proportional bias, respectively. Similarly, y-intercepts for A-B HDF and L-

S HDF were 4.82 and 0.69, respectively, which are very close to the origin (0.00), indicating no systematic bias. On the other hand, the one of the Impulse Angle was 21.1, which indicates a minimal systematic bias.

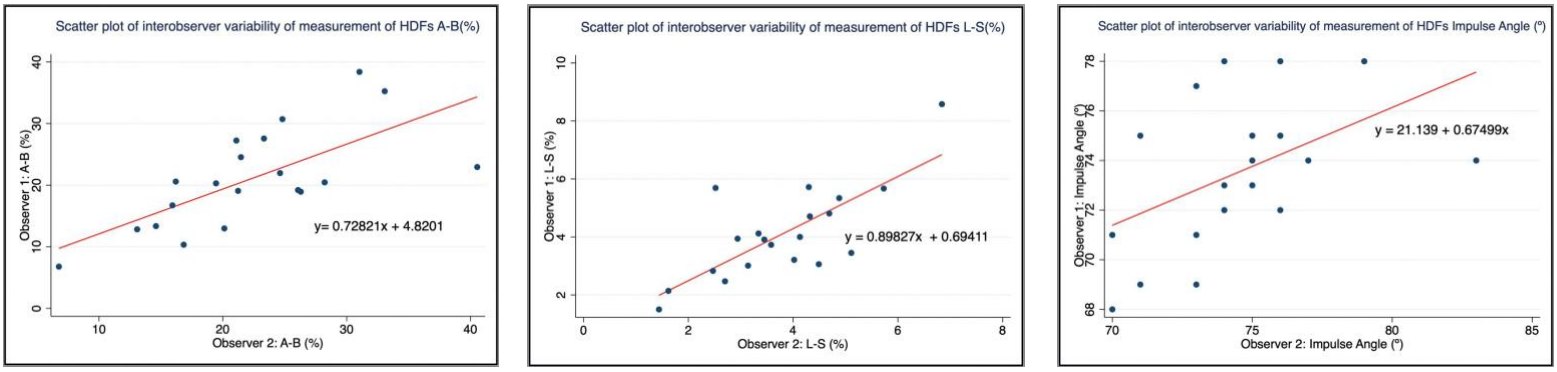

A **B** **C**

Figure 3

Scatter plots of correlation between the two observers of the longitudinal (A-B) HDF (Panel A), transverse (L-S) HDF (Panel B), and the impulse angle (Panel C).

For the HDF parameters, the bias trend can be visualized in **Figure 4** which shows Bland-Altman plots of agreement between the measurements of the two observers. While the x-axis shows the average of the two measurements, the y-axis shows the difference of the measurement between the two observers. Ideally, for the bias to be minimal, the y-values should approach zero. The middle line of agreement (red line) illustrates this concept. In all of the graphs for the three HDF parameters, the middle line of agreement is nearly at zero. The upper and lower limits of agreement, on the other hand, show the appropriate range for difference or bias between the two observer measurements. In each graph, one outlier was consistently found. This leads to the interpretation that two observers got close enough in 19 out of 20 CMR studies or 95%, which is considered to be accurate.

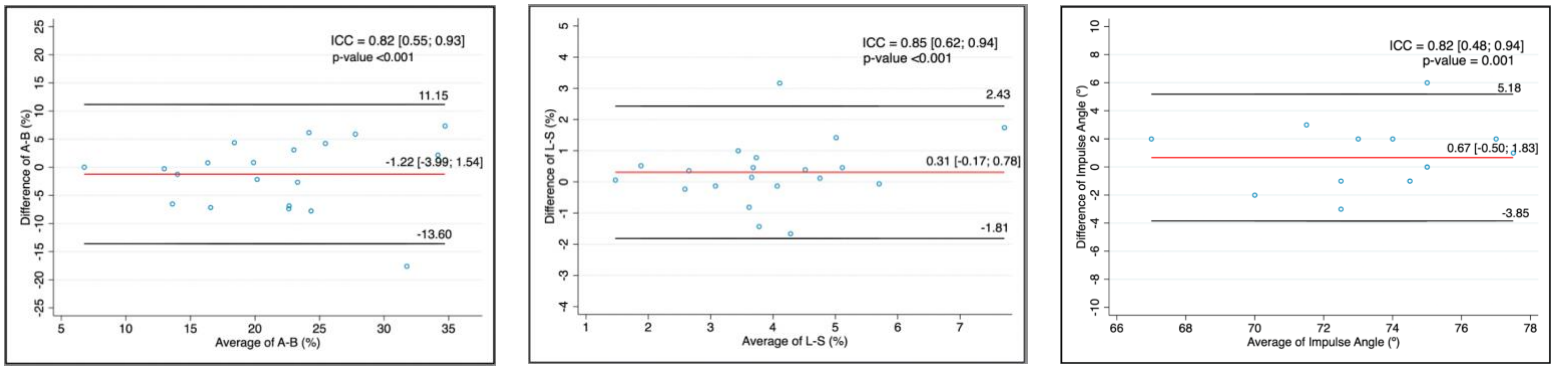

A **B** **C**

Figure 4

Bland-Altman plots of agreement between the two observers of the longitudinal (A-B) HDF (Panel A), transverse (L-S) HDF (Panel B), and the impulse angle (Panel C).

Intra-observer variability

Volumetric, valve diameter, and HDF parameters for 15 endurance athletes are shown in **Table 3**. First, it is important to highlight only a few parameters: LV ejection fraction in % (LVEF), aortic and mitral valve diameters in mm, Endo-Global Longitudinal Strain in %. Looking at the mean LVEF (62.4 ± 8.0), this value can be interpreted as clinically normal. Comparing the readings of the two observers, using Pearson's correlation test, a very strong correlation (r-value=0.97) and great significance (p-value <0.001) were found.

Meanwhile, the aortic valve area ICC value and p-value (0.80 and 0.003) shows a quite good correlation and quite good significance similar to those of the mitral valve (0.77 and 0.004). Furthermore, the ICC value and p-value of GLS-endo (0.95 and <0.001 respectively) showed even better results.

Albeit, the most important parameters for analysis were the HDF parameters for the entire heart cycle. Overall, the ICC values for A-B , L-S, and Impulse Angle showed excellent correlation and high statistical significance (0.89, 0.93, and 0.82, respectively; p<0.001 for all the parameters).

Looking at **Figure 5** showing scatter plots of correlation between the same HDF parameters, the x-axis and the y-axis show observer 1 measurements one week apart. The correlation between these measurements can be judged by the general pattern of the data points, which all created a clear pattern of correlation for all three HDF parameters through the noticeable line of best fit. While the slope for the A-B HDF is 0.96 and the slope for the L-S HDF is 0.97, the one for the Impulse Angle is 0.75. These results indicate no proportional bias and minimal proportional bias, respectively. Similarly, y-intercepts for A-B HDF and L-S HDF are 1.55 and 0.02, which are very close to the origin (0.00), indicating no constant systematic bias. On the other hand, that of the Impulse Angle is 18.6, which suggests minimal constant systematic bias.

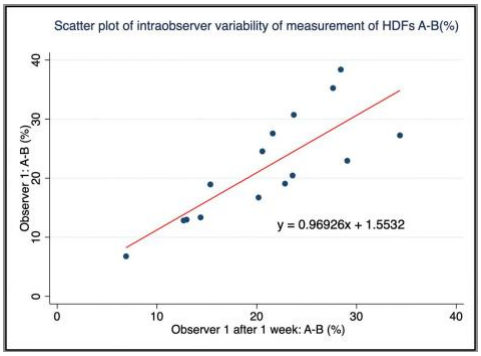

A

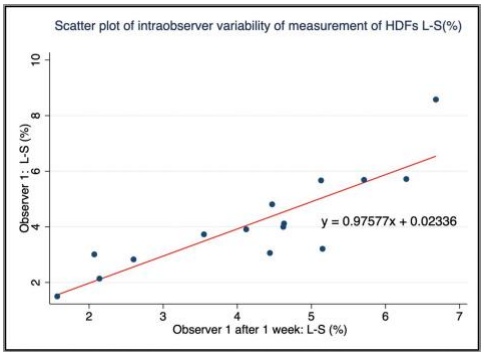

B

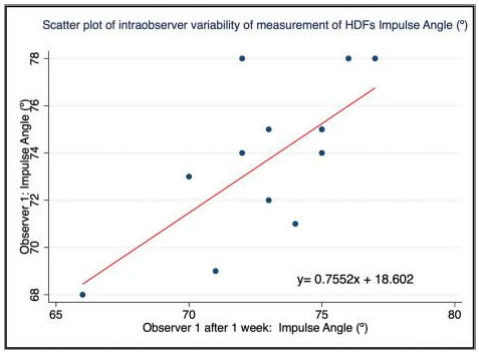

C

Figure 5

Scatter plots of correlation in repeated measurements by the same observer of the longitudinal (A-B) and transverse (L-S) HDF, and the impulse angle.

For these highlighted HDF parameters, the bias trend can be visualized on **Figure 6** showing Bland-Altman plots of agreement between two observer measurements. While the x-axis shows the average chosen parameter, the y-axis shows the difference in the measurement of this parameter by the two observers. Ideally, for the bias to be minimal, the y-values should approach zero. The middle line of agreement (red line) illustrates this phenomenon. Throughout all three graphs for these HDF parameters, the middle line of agreement is nearly at zero in terms of the y-axis. The upper and lower bounds of agreement, on the other hand, show the appropriate range for difference or bias between two observer measurements. In two of the three graphs, one outlier was consistently found. This leads to the interpretation that two observers may get close enough numbers 19/20 times or 95%, which is considered to be accurate.

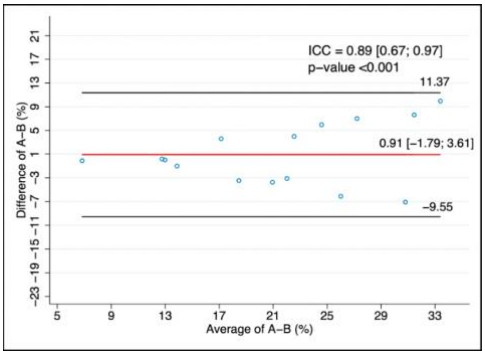

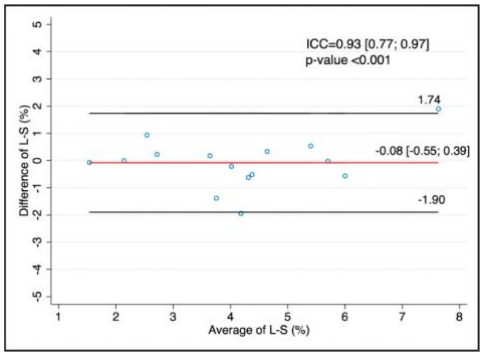

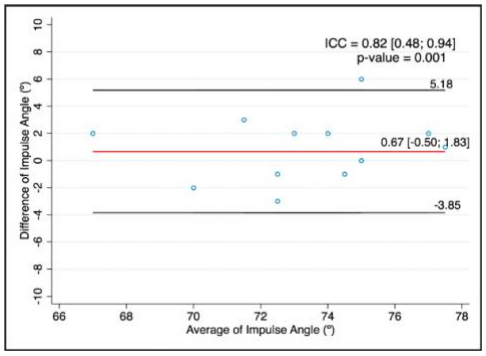

A **B** **C**

Figure 6

Bland-Altman plots of agreement in repeated measurements by the same observer of the longitudinal (A-B) and transverse (L-S) HDF, and the impulse angle.

Discussion

It is important to check inter- and intra-observer variability of HDF derived from feature tracking CMR since data on the reproducibility is scanty and any new method requires a statistical backing in terms of reproducibility to understand the acceptable HDF parameters variability range, if repeated.

Statistical Analysis

The Intra Class Coefficient (ICC) was used to evaluate the reproducibility of measurements made by two different observers (inter-observer variability) and the same observer one week apart (intra-observer variability). Considering the complex pairing of the data and looking out for systematic differences, this statistical method was preferred over Spearman's coefficient. The ICC was presented in the form of numerical difference and error of our paired data, where ICC values in the 0.75-1.00 range suggested excellent correlation, and those in the 0.60-0.74 indicated good correlation (Bunting, et al., 2019).

Scatter plots were created to visualize the correlation for the measurements of inter- and intra- observer variability. The regression analysis represented by a line of best fit should ideally mimic the line of equality (plotted as an equal diagonal line) in order to show strong correlation.

Bland-Altman plots were created in order to visualize the degree of agreement between different inter- and intra-observer measurements, to quantify numerical bias, and to depict potential data outliers. If the data points lie between the upper and lower limits of agreement, this indicates a good agreement. Also, a middle line of agreement close to zero represents a low bias.

Considering a normal distribution of the data, paired t-test was performed to look at the bias in the difference of paired data measurements. A p-value <0.05 was considered statistically significant.

Summary of the results

The findings of this study indicate that in a group of athletes undergoing CMR, HDF parameters showed high reproducibility.

In terms of inter-observer variability, the scatter plots showed a good correlation for all the HDF parameters. While A-B and L-S HDF showed no bias, the Impulse Angle measurements presented minimal systematic and proportional bias (**Figure 2, panel C**). The Bland-Altman plots for the three HDF parameters showed no bias since the midlines of agreement were close to zero and the upper/lower limits of agreement covered 95% of the measurements (**Figure 3**).

Looking at intra-observer variability, the scatter plots and the Bland-Altman plots showed similar positive results. Though, there was minimal systematic and proportional bias between Impulse Angle measurements made by the same observer one week apart (**Figure 4, panel C**).

Comparison with previous studies

There are only a few studies on the clinical application of HDF analysis: (Vos et al., 2023), (Ferrara et al., 2021), (Monosilio et al., 2022). **Table 4** summarizes the results of these studies and compares them with this study's results.

The study by (Vos et al., 2023) used the same approach as our study in patients with pulmonary hypertension; however, they looked into different parameters, according to the different cardiac phases (systolic ejection, systo-diastolic transition, and the passive and active filling), while we considered HDF throughout the entire cardiac cycle.

(Ferrara et al., 2021) reported HDF values in healthy individuals using echocardiography. Although several HDF parameters were measured, inter- and intra-observer variability is reported for longitudinal HDF over the whole cardiac cycle. Compared to our results, they found a higher inter- and intra-observer reproducibility (ICC 0.97 vs 0.82 and 0.98 vs 0.89, respectively).

More recently, (Monosilio et al., 2022) studied a group of patients with heart failure using echocardiography and the same software we have used in our study. Compared to those values, our results showed similar inter-observer, but higher intra-observer variability.

Potential sources of variability

Our study aimed to evaluate the variability of HDF parameters in athletes and to elucidate the potential sources of variability according to the different steps of analysis, which include: appropriate view selection, cardiac frame selection, endocardial border detection (EBD), and valve diameter measurement (**Table 5**).

For the cardiac frame selection, a minor source of variability was found. In fact, a difference of ≤2 frames between the two observers was present in 92% of the cases and in 100% of the cases re-analysed by the same observer one week apart.

Looking at the EBD step, the GLS shows excellent correlation and statistical significance, which is a consequence of the automatic function of EBD. The observers reported that they had to manually adjust the endocardial borders only in 1/20 patients. From this result, we believe that the software can be heavily trusted for follow-up studies.

In terms of the valve diameter measurement, our results indicate a slightly lower correlation for the aortic valve area compared with mitral valve measurements (**Table 2**). This finding could be explained by the cylinder-like shape of the LVOT, with different diameters at different levels, and by the lack of anatomical landmarks, which could potentially result in different diameter selection by the operator(s). In contrast, mitral valve annulus has definite hinge points which the operator can use as a gold reference to measure the mitral valve diameter.

Overall, we would like to emphasize the importance of joint training sessions using software analysis for reducing the degree of variability. Even with experience in cardiac imaging, there should be some agreement on the standardization of measurements.

Thus, based on our experience, view selection and valve area measurements are the most challenging steps in terms of reproducibility, while frame selection and endocardial border detection are much less operator-dependent (**Table 5**).

Limitations

Despite the low variability in the observer measurements, there are some aspects that must be considered. Firstly, the software program only allows the rounding down to one decimal place for the diameter of the valves. Secondly, the measurement of the mitral valve at the annulus and the aortic valve at the LVOT may not reflect the actual area in which the blood flows. Lastly, it is not clear if observers with less than 6 years of experience in cardiac imaging will achieve the same degree of reproducibility as found in our study.

Conclusions

The results of this study show a low inter- and intra-observer variability for the analysis of HDF parameters using CMR images. Image view selection and valve area measurements are the most vulnerable steps in terms of reproducibility of this method. These findings will likely open new avenues for this method for wide application in clinical settings, in particular for patients undergoing follow-up studies and for early detection of cardiac dysfunction.

Acknowledgments

Special thanks to radiology senior nurse Gulmira Ayapergenova for athletes' CMR scheduling, physicist Yesimzhan Raiymbekov and radiology technician Aizhan Zhanbolatova for technical support.

References

1. Airale, L., Vallelonga, F., Forni, T., Leone, D., Magnino, C., Avenatti, E., ... & Milan, A. (2021). A novel approach to left ventricular filling pressure assessment: the role of hemodynamic forces analysis. *Frontiers in Cardiovascular Medicine*, *8*, 704909.

2. Anvari, A., Halpern, E. F., & Samir, A. E. (2018). Essentials of statistical methods for assessing reliability and agreement in quantitative imaging. *Academic radiology*, *25*(3), 391-396.

3. Bunting, K. V., Steeds, R. P., Slater, L. T., Rogers, J. K., Gkoutos, G. V., & Kotecha, D. (2019). A practical guide to assess the reproducibility of echocardiographic measurements. *Journal of the American Society of Echocardiography*, *32*(12), 1505-1515.

4. Claus, P., Omar, A. M. S., Pedrizzetti, G., Sengupta, P. P., & Nagel, E. (2015). Tissue tracking technology for assessing cardiac mechanics: principles, normal values, and clinical applications. *JACC: Cardiovascular Imaging*, *8*(12), 1444-1460.

5. Demark-Wahnefried, W., Morey, M. C., Sloane, R., Snyder, D. C., Miller, P. E., Hartman, T. J., & Cohen, H. J. (2012). Reach out to enhance wellness home-based diet-exercise intervention promotes reproducible and sustainable long-term improvements in health behaviors, body weight, and physical functioning in older, overweight/obese cancer survivors. *Journal of Clinical Oncology*, *30*(19), 2354.

6. Doost, S. N., Ghista, D., Su, B., Zhong, L., & Morsi, Y. S. (2016). Heart blood flow simulation: a perspective review. *Biomedical engineering online*, *15*, 1-28.

7. Eriksson, J., Bolger, A. F., Ebbers, T., & Carlhall, C. J. (2015). Left ventricular hemodynamic forces are altered in patients with dilated cardiomyopathy. *Journal of Cardiovascular Magnetic Resonance*, *17*(1), 1-2.

8. Ferrara, F., Capuano, F., Cocchia, R., Ranieri, B., Contaldi, C., Lacava, G., ... & Bossone, E. (2021). Reference ranges of left ventricular hemodynamic forces in healthy adults: a speckle-tracking echocardiographic study. *Journal of clinical medicine*, *10*(24), 5937.

9. Filomena, D., Cimino, S., Monosilio, S., Galea, N., Mancuso, G., Francone, M., ... & Agati, L. (2022). Impact of intraventricular haemodynamic forces misalignment on left ventricular remodeling after myocardial infarction. *ESC Heart Failure*, *9*(1), 496-505.

10. Flachskampf, F. A., Biering-Sørensen, T., Solomon, S. D., Duvernoy, O., Bjerner, T., & Smiseth, O. A. (2015). Cardiac imaging to evaluate left ventricular diastolic function. *JACC: Cardiovascular Imaging*, *8*(9), 1071-1093.

11. Herzog, B., Greenwood, J., Plein, S., Garg, P., Haaf, P., Onciul, S. (2017). Cardiovascular Magnetic Resonance Pocket Guide. *European Society of Cardiology & European Association of Cardiovascular Imaging*

12. Hove, J. R., Köster, R. W., Forouhar, A. S., Acevedo-Bolton, G., Fraser, S. E., & Gharib, M. (2003). Intracardiac fluid forces are an essential epigenetic factor for embryonic cardiogenesis. *Nature, 421(6919), 172-177.*

13. Ortaliza, J., Amin, K., Cox, C. (2022). COVID-19 leading cause of death ranking. https://www.healthsystemtracker.org/brief/covid-19-leading-cause-of-death-ranking/#Total%20deaths%20in%20the%20United%20States%20from%20COVID-19%20and%20other%20leading%20causes,%202020-2022

14. Koo, T. K., & Li, M. Y. (2016). A guideline of selecting and reporting intraclass correlation coefficients for reliability research. *Journal of chiropractic medicine*, *15*(2), 155-163.

15. Laenens, D., van der Bijl, P., Stassen, J., Rossi, A. C., Pedrizzetti, G., Reiber, J. H., ... & Bax, J. J. (2023). Introduction to hemodynamic forces by echocardiography. *International Journal of Cardiology*, *370*, 442-444.

16. Meesters, A. M., Ten Duis, K., Banierink, H., Stirler, V. M., Wouters, P. C., Kraeima, J., ... & IJpma, F. F. (2020). What are the interobserver and intraobserver variability of gap and stepoff measurements in acetabular fractures?. *Clinical Orthopaedics and Related Research*, *478*(12), 2801.

17. Midgett, M., & Rugonyi, S. (2014). Congenital heart malformations induced by hemodynamic altering surgical interventions. *Frontiers in physiology*, *5*, 287.

18. Monosilio, S., Filomena, D., Luongo, F., Sannino, M., Cimino, S., Neccia, M., ... & Agati, L. (2022). Cardiac and vascular remodeling after 6 months of therapy with sacubitril/valsartan: mechanistic insights from advanced echocardiographic analysis. *Frontiers in Cardiovascular Medicine*, *9*.

19. Olivetti, G., Anversa, P., & Loud, A. V. (1980). Morphometric study of early postnatal development in the left and right ventricular myocardium of the rat. II. Tissue composition, capillary growth, and sarcoplasmic alterations. *Circulation research*, *46*(4), 503-512.

20. Pedrizzetti, G., Claus, P., Kilner, P. J., & Nagel, E. (2016). Principles of cardiovascular magnetic resonance feature tracking and echocardiographic speckle tracking for informed clinical use. *Journal of cardiovascular magnetic resonance*, *18*(1), 1-12.

21. Pedrizzetti, G., Martiniello, A. R., Bianchi, V., D'Onofrio, A., Caso, P., & Tonti, G. (2016). Changes in electrical activation modify the orientation of left ventricular flow momentum: novel observations using echocardiographic particle image velocimetry. *European Heart Journal-Cardiovascular Imaging*, *17*(2), 203-209.

22. Pedrizzetti, G., Martiniello, A. R., Bianchi, V., D'Onofrio, A., Caso, P., & Tonti, G. (2015). Cardiac fluid dynamics anticipates heart adaptation. *Journal of Biomechanics*, *48*(2), 388-391.

23. Peng, P., Lekadir, K., Gooya, A., Shao, L., Petersen, S. E., & Frangi, A. F. (2016). A review of heart chamber segmentation for structural and functional analysis using cardiac magnetic resonance imaging. *Magnetic Resonance Materials in Physics, Biology and Medicine*, *29*, 155-195.

24. Popović, Z. B., & Thomas, J. D. (2017). Assessing observer variability: a user's guide. *Cardiovascular diagnosis and therapy*, *7*(3), 317.

25. Reddy, K., Khaliq, A., & Henning, R. J. (2015). Recent advances in the diagnosis and treatment of acute myocardial infarction. *World journal of cardiology*, *7*(5), 243.

26. Shiran, A., Adawi, S., Ganaeem, M., & Asmer, E. (2009). Accuracy and reproducibility of left ventricular outflow tract diameter measurement using transthoracic when compared with transesophageal echocardiography in systole and diastole. *European Journal of Echocardiography*, *10*(2), 319-324.

27. Sund-Levander, M., Grodzinsky, E., Loyd, D., & Wahren, L. K. (2004). Errors in body temperature assessment related to individual variation, measuring technique and equipment. *International journal of nursing practice*, *10*(5), 216-223.

28. Szulik, M., Pappas, C. J., Jurcut, R., Magro, M., Peeters, E., Goetschalckx, K., ... & Voigt, J. U. (2011). Clinical validation of a novel speckle-tracking–based ejection fraction assessment method. *Journal of the American Society of Echocardiography*, *24*(10), 1092-1100.

29. Thomas, J. D., & Popović, Z. B. (2005). Intraventricular pressure differences: a new window into cardiac function. *Circulation*, *112*(12), 1684-1686.

30. Vallelonga, F., Airale, L., Tonti, G., Argulian, E., Milan, A., Narula, J., & Pedrizzetti, G. (2021). Introduction to hemodynamic forces analysis: moving into the new frontier of cardiac deformation analysis. *Journal of the American Heart Association*, *10*(24), e023417.

31. Vos, J. L., Leiner, T., van Dijk, A. P., Pedrizzetti, G., Alenezi, F., Rodwell, L., ... & Nijveldt, R. (2023). Cardiovascular magnetic resonance-derived left ventricular intraventricular pressure gradients among patients with precapillary pulmonary hypertension. *European Heart Journal-Cardiovascular Imaging*, *24*(1), 78-87.

Appendix

Table 1.

General characteristics of the 20 athletes.

Parameter	**Total (n=20)**
Age, years (SD)	30.0 (9.1)
Gender, n (%)	
Female	10 (50.0)
Male	10 (50.0)
Weight, kg (SD)	66.6 (15.2)
Height, cm (SD)	169.5 (9.3)
BSA, m^2 (SD)	1.76 (0.24)
HR, bpm (SD)	65.5 (13.9)
SBP, mmHg (SD)	112.3 (13.0)
DBP, mmHg (SD)	74.4 (8.9)
MAP, mmHg (SD)	87.0 (10.0)
Sport experience, years (SD)	11.4 (8.3)

BSA, Body Surface Area; DBP, diastolic blood pressure; HR, heart rate; MAP, mean arterial pressure; SBP, systolic blood pressure.

Table 2.

Inter-observer variability for volumetric, valve diameters, feature tracking analysis, and HDF parameters.

Parameter	Observer 1 (n=20)	Observer 2 (n=20)	Correlation	p-value	Statistical test
Volumetric					
LVEF, % (SD)	62.3 (7.3)	63.0 (4.6)	r=0.88	<0.001	Pearson's correlation
LVESV, mL (SD)	56.7 (21.3)	54.8 (18.5)	r=0.90	<0.001	
LVESVi, mL/m^2 (SD)	32.1 (11.7)	30.8 (8.7)	r=0.89	<0.001	
LVEDV, mL (SD)	147.9 (41.3)	146.8 (37.7)	r=0.98	<0.001	
LVEDVi, mL/m^2 (SD)	83.9 (21.4)	83.2 (18.3)	r= 0.98	<0.001	
SV, mL (SD)	91.2 (25.7)	92.0 (21.2)	r=0.93	<0.001	
SVi, mL/m^2 (SD)	51.8 (13.9)	52.3 (11.2)	r=0.90	<0.001	
Valve diameters					
Aortic valve, mm (SD)	22.8 (3.2)	21.6 (1.9)	ICC= 0.68 (0.49-0.87)	0.01	ICC
Mitral valve, mm (SD)	32.8 (3.3)	36.2 (3.1)	ICC=0.82 (0.62 -0.98)	<0.001	
Feature tracking analysis					
GLS-endo, % (SD)	-25.1 (5.2)	-25.3 (4.5)	ICC =0.89 (0.73-0.95)	<0.001	ICC
GCS-endo, % (SD)	-30.3 (4.4)	-30.7 (3.2)	ICC= 0.82 (0.55-0.93)	0.005	
Hemodynamic forces					
A-B, % (SD)	21.0 (5.2)	22.2 (7.6)	ICC = 0.82 (0.55-0.93)	<0.001	ICC
L-S, % (SD)	4.0 (1.6)	3.7 (1.3)	ICC=0.85 (0.62 -0.94)	<0.001	
Impulse angle, º (SD)	73.5 (2.9)	74.5 (3.0)	ICC=0.67 (0.15- 0.86)	0.012	

Table 3.

Intra observer variability for volumetric, valve diameter, feature tracking analysis, and HDF parameters.

Parameter	Observer 1 (n=15)	Observer 1 after 1 week (n=15)	Correlation	p-value	Performed test
Volumetric					
LVEF, % (SD)	62.4 (8.0)	62.8 (8.4)	r=0.97	<0.001	Pearson's correlation
LVESV, mL (S)	57.4 (22.7)	56.3 (20.6)	r=0.97	<0.001	
LVESVi, mL/m^2 (SD)	32.2 (12.6)	31.6 (11.6)	r=0.96	<0.001	
LVEDV, mL (SD)	149.6 (43.9)	149.1 (38.6)	r=0.97	<0.001	
LVEDVi, mL/m^2 (SD)	84.2 (23.4)	83.3 (19.6)	r=0.97	<0.001	
SV, mL (SD)	92.1 (27.7)	92.7 (25.7)	r=0.97	<0.001	
SVi, mL/m^2 (SD)	51.9 (15.5)	52.1 (13.9)	r=0.97	<0.001	
Valve diameter					
Aortic valve, mm (SD)	22.6 (3.2)	22.7 (2.6)	ICC= 0.80 (0.49-0.93)	0.003	ICC
Mitral valve, mm (SD)	33.7 (3.2)	32.6 (3.8)	ICC=0.77 (0.55 -0.92)	0.004	
Strain					
GLS-endo, % (SD)	-25.9 (5.6)	-25.7 (6.1)	ICC =0.95 (0.84-0.98)	<0.001	ICC
GCS-endo, % (SD)	-30.0 (4.5)	-30.6 (4.6)	ICC= 0.92 (0.77 -0.97)	<0.001	
Hemodynamic forces					
A-B, % (SD)	21.8 (8.8)	20.9 (7.4)	ICC = 0.89 (0.67-0.97)	<0.001	ICC
L-S, % (SD)	4.1 (1.7)	4.2 (1.5)	ICC=0.93 (0.77 -0.97)	<0.001	
Impulse angle, º (SD)	73.9 (3.0)	73.2 (2.7)	ICC=0.82 (0.48- 0.94)	0.001	

Table 4.

Inter- and intra-observer variability of HDF parameters: comparison with previous studies.

Reference	Imaging	Parameters	Inter-obs. ICC (95% CI)	p-value	Intra-obs. ICC (95%)	p-value	Population
Vos et al., 2023	CMR	IVPG:					
		"A"	0.81 (0.52-0.93)	<0.001	0.75 (0.40-0.91)	<0.001	Pulmonary
		"B"	0.88 (0.67-0.96)	<0.001	0.94 (0.82-0.98)	<0.001	Hypertension
		"C"	0.87 (0.65-0.95)	<0.001	0.94 (0.82-0.98)	<0.001	
		"D"	0.94 (0.84-0.98)	<0.001	0.99 (0.96-1.00)	<0.001	
Ferrara et al., 2021	Echo	HDF:					
		Amplitude	0.97 (0.93-0.98)	<0.01	0.98 (0.95-0.99)	<0.01	Healthy
		Heartbeat					
		Longitudinal					
Monosilio et al., 2022	Echo	HDF:					
		A-B	0.85 (0.36-0.96)	0.006	0.82 (0.22-0.96)	0.014	Heart Failure
		L-S	0.87 (0.14-0.97)	0.001	0.76 (0.01-0.94)	0.030	
		L-S/A-B	0.76 (0.06-0.94)	0.018	0.79 (0.06-0.95)	0.024	
Present study	CMR	HDF:					
		A-B	0.82 (0.67-0.97)	<0.001	0.89 (0.67-0.97)	<0.001	
		L-S	0.85 (0.62 -0.94)	<0.001	0.93 (0.77 -0.97)	<0.001	Athletes
		Impulse Angle	0.67 (0.15- 0.86)	0.012	0.82 (0.48- 0.94)	0.001	

Echo, Echocardiography; obs, observer; "A", Systolic ejection force; "B", Downward force at systolic-diastolic transition; "C", E-wave decelerative force; "D", A-wave Acceleration

Table 5.

Summary of HDF analysis steps and their relative degree of variability, where (+++) is the highest and (- - -) is the lowest variability.

Step	**Variability**
View Selection	+ + +
Frame Selection	+ / - -
Endocardial Border Detection	- - -
Valve Area	+ + / -